Mass transfer in SiO$_2$ nanofluids: A case against purported nanoparticle convection effects

Xuemei Feng, Drew W. Johnson *

Department of Civil & Environmental Engineering, University of Texas at San Antonio, San Antonio, TX 78249, USA

ARTICLE INFO

ABSTRACT

Controversy and the ambiguity exist in the scientific literature for the question of if nanoparticles truly enhance heat and mass transfer. This study experimentally explored effects of non-aggregating spherical SiO$_2$ nanoparticles on oxygen and NaCl mass transfer. No mass transfer enhancements were found in the presence of nanoparticles. Oxygen transfer was actually diminished at the highest nanoparticle volume fraction; this is attributed to solution viscosity effects and the obstruction effects of impermeable nanoparticles. No evidence was found to substantiate the purported Brownian motion micro/nano-scale convection effect of nanoparticles that has been used by others to explain anomalous heat and mass transfer rates in nanofluids.

1. Introduction

Prior studies have shown nanofluids, the suspension of 1–100 nm nanoparticles in fluids including water, engine oil and ethylene glycol, can enhance the thermal conductivities of mixtures, and the enhancements are anomalously larger than those predicted by effective medium theory [1–6]. The phenomena of measured thermal conductivity out of the effective medium theory prediction ranges have been repeated and explored in numerous follow-up studies as summarized in topical review Refs. [7–11]. Additional studies have examined nanoparticle effects on mass transfer and mass diffusivity in nanofluids [12–20]; results from these studies are provided in Table 1 in chronological order. Mass transfer enhancements in nanofluids are reported for a variety of nanoparticle types and nanoparticle concentration ranges, with the highest enhancement found for carbon dioxide mass transfer, 48 times greater into water when in the presence of 1% volume fraction of iron oxide nanoparticles [18]. These mass transfer enhancements are usually interpreted as resulting from enhanced mass diffusivities. For studies that have attempted to measure mass diffusivities directly, a majority of studies report diffusivity enhancements. The greatest diffusivity enhancement was found by Fang et al. [17], who report that the diffusion coefficient of Rhodamine B in 0.5% Cu–water nanofluid is 26 times larger than that in de-ionized water at 25 °C. Not all published studies support diffusivity enhancements in nanofluids. Using nuclear magnetic resonance (NMR) methods, Turanov and Tolmachev [16] found a

decrease in proton self diffusion in nanofluids, and Ozturk et al. [19] argue that the anomalous enhancement for diffusivities determined from dye diffusion [13,17] is due to complexation interactions between the dye and nanoparticles. When minimization of interactions between dye and nanoparticles were achieved, Ozturk et al. [19] showed that Al$_2$O$_3$ nanoparticles do not enhance dye diffusion. In contrast, Veilleux and Coulombe [20] also minimized dye and nanoparticles interaction but still found a 10 times larger dye diffusion in Al$_2$O$_3$ nanofluids. Aside from the diffusivity measurement studies, scant published studies exist which report no mass transfer enhancement for nanofluids. Brownian motion is one mechanism adopted to explain anomalous enhancements. Brownian motion of nanoparticles is purported to create micro/nano-scale convection to increase both heat and mass transfer [13,17,21,22]. However, this explanation is controversial as the nanoparticle induced micro/nano-scale convection is poorly characterized. Furthermore, recent studies argue that nanoparticles cannot enhance mass transfer [16,19], and that heat transfer enhancements can be predicted with effective medium theory [16,23,24]. While the effective medium theory may be used to explain heat transfer enhancements, it does not apply for mass transfer enhancement.

Given the ambiguity of if nanoparticles truly increase heat and mass transfer, further experimental data are necessary to clarify the enhancements and purported associated Brownian motion effects. Diffusion cells measurements are the classical method for determining diffusion coefficients [25,26]. In this study, oxygen and NaCl mass transfer in a diffusion cell containing nanofluid are investigated. The oxygen transfer study explores the Brownian motion effect under an interfacial mass transfer scenario. The NaCl

* Corresponding author. Tel.: +1 210 458 5513; fax: +1 210 458 6475.
E-mail address: Drew.Johnson@UTSA.edu (D.W. Johnson).

Nomenclature

A_p	membrane pore area (mm^2)
C_{High} C_{Low}	high concentration, low concentration (mg/L)
C_{ht}, C_{h0}, C_{lt}, C_{l0}	high concentration at time t, 0, low concentration at time t, 0
C_0	time zero oxygen concentration (mg/L)
C_s	saturated oxygen concentration (mg/L)
ΔC_0, ΔC_t	cell concentration differences at time 0 and t (mg/L)
C_{so}	saturated oxygen concentration of nanoparticle free control (mg/L)
C_{sp}	saturated oxygen concentration with nanoparticles present (mg/L)
C_t	oxygen concentration at time t (mg/L)
d	star-head magnetic stir bar diameter (cm)
D, D_M	diffusivity, density driven measured diffusivity (m^2/s)
D_{eff}, D_{NaCl}	effective diffusivity, NaCl mass diffusivity (m^2/s)
d_p	membrane pore diameter (μm)
g	gravitational acceleration (m/s^2)
K	polycarbonate membrane permeability (m^2)
K_L	liquid film mass transfer coefficient, (m/s)
K_La	volumetric mass transfer coefficient (1/min)
n	pore density (pores/cm^2)
Pe	Peclet number, dimensionless
Re	Reynolds number, dimensionless
R_b, R_T	boundary resistance, total resistance (min/cm)
Sc	Schmidt number, dimensionless

Sh	Sherwood number, dimensionless
t	time (min)
V	total volume of solution (mL)
v	velocity

Greek symbols

δ_b, δ_m	boundary thickness, membrane thickness (μm)
μ	dynamic solution viscosity (mPa·s)
ρ	solution density (g/mL)
$\Delta\rho$	density difference (g/mL)
ϕ	volume fraction (%)

Subscripts

0	0 time
b	boundary
eff	effective
ht, $h0$, lt, $l0$	high and low concentration cell at time is t and 0
L	liquid film
m	membrane
M	measured
p	pore
so	saturated free of nanoparticles
sp	saturated with nanoparticles
t	t time
T	total

transfer incorporates transfer across a liquid embedded membrane and explores nanofluid effect on diffusive transfer in an alternative scenario; one not incorporating a gas liquid interface.

2. Experimental methods

2.1. Nanoparticle characterization

The nanoparticles used in this study are spherical SiO$_2$ nanoparticles (nominal size 13.7 ± 2 nm and 22.5 ± 2.5 nm, Microspheres–Nanospheres, Cold Springs, NY, 149011-05, 149015-05). Diameters of nanoparticles used were measured using a dynamic light scattering method through Delsa Nano C (Beckman Coulter Inc, Brea, CA) with 658 nm laser and scattering angle 165°. The measured diameters in NaCl mass transfer study were 17.2 ± 1.0 and 22.5 ± 1.5 nm. For the oxygen mass transfer study, measured diameters were 20.0 ± 1.1 and 24.5 ± 2.4 nm. Measured nanoparticle sizes did not change after thirty-four hours of incubation in the experimental conditions used, and sizes were stable over the duration of the experiments. Nanoparticle size differences between the oxygen transfer study and the NaCl study may be due to different batches used from the manufacturer and also storage time differences between uses.

2.2. Adsorption assessment

Adsorption tests were conducted to verify that the membrane and nanoparticles were non-interacting with the chloride. For membrane adsorption measurements, 13 mm circular polycarbonate membranes (Membrane solutions, Plano, TX, MFPC013040) were placed in 40 mL borosilicate glass vials containing 5.2 mL of 0.01, 0.025, 0.05 and 0.1 M NaCl. NaCl solutions were made by dissolving desired amounts of ACS grade NaCl (Thermo Fisher Scientific Inc., Pittsburgh, PA, 7647-14-5) into nanopure water of resistivity 18.2 MΩ·cm. For nanoparticle adsorption assessment, 5.2 mL of 0.5% nanofluid was prepared at the same NaCl concentrations. The concentration of chloride was recorded using a calibrated ion selective electrode (ISE) (Thermo Fisher Scientific Inc., Pittsburgh, PA, 13-620-527) at the beginning of the experiment, and after shaking at 70 rpm for 50 h at 25 °C.

2.3. Diffusion cell measurements

The membrane diffusion cell (PermeGear Inc., Hellertown, PA) used is depicted in Fig. 1. The cell was used to measure the mass transfer rate of NaCl through SiO$_2$-water nanofluid embedded within 0.4 μm pores of a track etched polycarbonate membrane.

Table 1
Summary of reported nanofluid mass transfer effects.

| Investigators	Nanofluid type	Experimental method	Particle volume fraction unless indicated	Enhancement ratio
Kim et al., 2006 [12]	Cu/H$_2$O	Ammonia absorption	0.01–0.1 wt%	3.2
	CuO/ H$_2$O			3
	Al$_2$O$_3$/ H$_2$O			3
Krishnamurthy et al., 2006 [13]	Al$_2$O$_3$/H$_2$O	Fluorescein dye diffusion	0.1–1%	14
Olle et al., 2006 [14]	Fe$_3$O$_4$/H$_2$O	Oxygen transfer	0.25–4 wt%	6
Zhu et al., 2008 [15]	MCM41/H$_2$O	Carbon monoxide mass transfer	0.05–0.4 wt%	1.9
Turanov and Tolmachev, 2009 [16]	SiO$_2$/H$_2$O	Self-diffusion coefficient of proton	3.8–23%	0.7 (reduction)
Fang et al., 2009 [17]	Cu/H$_2$O	Fluorescent Rhodamine B dye diffusion	0.1–0.5%	26
Komati and Suresh, 2010 [18]	Fe$_3$O$_4$/H$_2$O	Oxygen and carbon dioxide absorption	0.05–1%	48
Ozturk et al., 2010 [19]	Al$_2$O$_3$/H$_2$O	Fluorescent dye diffusion	0.25–1%	1.0 (no enhancement)
Veilleux and Coulombe, 2010 [20]	Al$_2$O$_3$/H$_2$O	Rhodamine 6G dye diffusion	0.1–4%	10
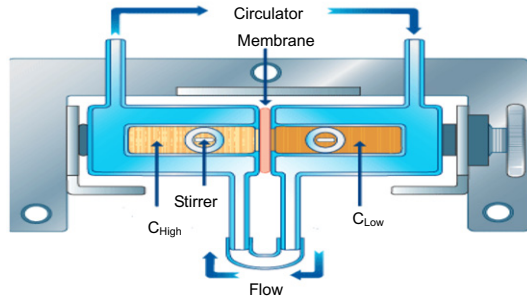
Fig. 1. Membrane diffusion cell configuration viewed from above, used with permission (PermeGear Inc., Hellertown, PA).

This membrane has a manufacturer reported porosity of 18.8%. Based on the modified form of Renkin's equation [27], the membrane pore size is large enough that the Brownian motion of nanoparticles present in the membrane pores are within approximately 90% of unhindered values. With this configuration, the NaCl diffusion path is depicted in Fig. 2, diffusion occurs through a liquid film adjacent to the membrane in the high concentration cell, through liquid filled pores of the membrane, and subsequently through the liquid film adjacent to the membrane in the low concentration cell. The diffusion cell is constructed of 6.5 mL glass half cells with 5 mm diameter circular throats on the clamping surfaces that sandwich the polycarbonate membrane. The half cells are mixed using 7 mm discs magnetically stirred at 600 rpm as verified with digital stroboscope (Ametek, Largo, FL, 1956) over the range of volume fractions studied. In order to obtain liquid tight sealing between the two half cells, petroleum jelly was added to edge of clamping surface between the cells. Each half cell contained two circular ports on the top of the diffusion cell; one 15 mm diameter opening for inserting the 13 mm chloride ISE and one 7 mm opening for fluid addition and sampling. Paraffin film (Thermo Fisher Scientific Inc., Pittsburgh, PA, 13-374-10) was used to seal sample ports and fitted probes to prevent the evaporation losses during mass transfer studies.

The mass transfer rate of NaCl across the membrane in the diffusion cell was evaluated by monitoring the change rate of chloride concentration in each half cell. Initial concentrations were at approximately 3000 ppm and 100 ppm in the high and low concentration half cells, respectively. To observe large concentration differences in both half cells, the concentrations were monitored using chloride ISEs over 9 h with data stored using a benchtop mul-
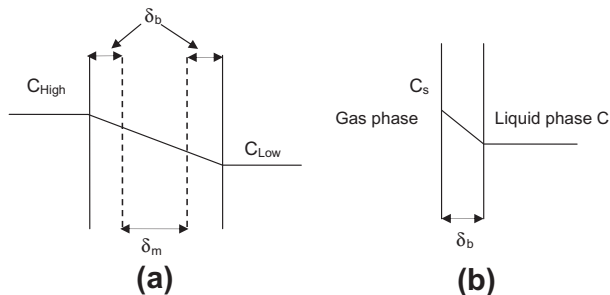
tiparameter meter (Thermo Fisher Scientific Inc., Pittsburgh, PA, 13-642-055). The mass transfer rate is transient as the concentrations change over time, but the transfer parameters are constant and can be determined experimentally. The overall NaCl mass transfer resistance (R_T) can be calculated using Eq. (1).

$$\ln \frac{\Delta C_t}{\Delta C_0} = -\frac{2A_p}{VR_T} t \tag{1}$$

where A_p is the pore area of the membrane (3.7 mm^2), V is the total volume of solution (5.2 mL), ΔC_0 and ΔC_t represent concentration differences between cells at initial and at measurement time t, respectively. R_T is the total mass transfer resistance provided by the membrane (the first term on the right hand side of Eq. (2)) and adjacent liquid film layers (R_b) on each side of the membrane [25].

$$R_T = \frac{\delta_m}{D_{NaCl} n\pi \left(\frac{d_p}{2}\right)^2} + 2R_b \tag{2}$$

where δ_m is thickness of membrane (25 μm), D_{NaCl} is NaCl mass diffusivity at temperature 25 °C , 1.6×10^{-9} m^2/s is taken [28] , d_p is membrane pore diameter (0.4 μm), n is pore density of 1.5×10^8 pores/cm^2, and 13.76 min/cm is calculated for membrane resistance. R_T is determined from the line of best fit slope when plotting $\ln(\Delta C_0/\Delta C_t)$ versus time and was determined in triplicate for nanoparticle concentrations of 0.5, 2.5 and 5 vol % at 25 ºC. The chloride ISEs used had manufacturer reported reproducibility of 2% and half-cell mass balances agreed within 2%. To account for potential interference of nanoparticles on probe readings, prior to the start of each measurement, the probes were calibrated in standard NaCl solutions that included equivalent nanoparticle concentrations used during the mass transfer measurements.

The side by side diffusion cell as utilized in this study facilitates ISE probe measurements. However, a drawback of this horizontal configuration is the potential for density differences and density-driven flow through the membrane interfering with concentration gradient mass transfer measurements. The relationship between true NaCl diffusivity (D_{NaCl}) and measured diffusivity (D_M) influenced by density-driven flow can be expressed as function of Peclet number (Pe) as shown in Eq. (3) [29].

$$D_M = D_{NaCl} \left(1 + \frac{Pe^2}{48}\right) \tag{3}$$

with

$$Pe = \frac{K(\Delta\rho)g d_p}{2\mu D_{NaCl}} \tag{4}$$

where, based upon manufacturer reported permeability, the Darcy permeability (K) of the polycarbonate membrane is of magnitude 10^{-15} m^2, d_p is the diameter of membrane pores (0.4 μm), g is gravitational acceleration, μ is solution dynamic viscosity (9.58×10^{-4} N S/m^2). In this study, the largest density difference ($\Delta\rho$) due to half cell NaCl concentration differences at the beginning of experiments is 2.5 kg/m^3. Pe is 1.2×10^{-8} and the effect of density-driven flow is negligible.

The oxygen mass transfer measurements did not involve transport through the membrane. Only half of the diffusion cell was used. The membrane was removed and the cell throat sealed with paraffin film. The same stirring arrangement described previously was used. Oxygen exchange from the atmosphere occurred at the air-nanofluid interface through the two ports of the half cell. As depicted in Fig. 2, the diffusion path incorporates only the liquid film at the air-nanofluid interface. The half cell probe port was fitted with a 12 mm diameter oxygen selective electrode (Hach, Loveland, CO, 5197000), calibrated daily according to manufacturer

Fig. 2. (a) Resistance to NaCl mass transfer. Transfer occurs from the high concentration cell (C_{High}) to the low concentration cell (C_{Low}) with passage through one liquid boundary layer of thickness of δ_b, a membrane of thickness δ_m and another liquid boundary layer of thickness δ_b. (b) Resistance to oxygen mass transfer. Transfer occurs from the gas phase at a saturated oxygen concentration C_s to liquid phase at an oxygen concentration C through a liquid boundary layer of thickness δ_b.

recommendations. For these oxygen transfer studies, nanopure water was deoxygenated with 1 g/L sodium sulfite and 1 mg/L $CoCl_2$ added to the cell.

For the oxygen transfer experiments, a volumetric mass transfer coefficient (K_La) (Eq. (5)), is calculated based on the oxygen concentration change rate, with initial dissolved oxygen concentration C_0, saturated dissolved oxygen concentration C_s, and dissolved oxygen concentration when time is t, C_t.

$$\ln\left(\frac{C_s - C_0}{C_s - C_t}\right) = K_L a t \qquad (5)$$

C_S is influenced by environmental conditions of barometric pressure and temperature. To account for slight variations in these conditions, C_S was determined for controls and individually for each treatment as the average C_t over a 20 min duration once C_t ceased to continuously increase for each nanoparticle volume fraction studied. K_La was determined in triplicate for nanoparticles of 20.0 ± 1.1 nm and 24.5 ± 2.4 nm at concentrations of 0.5, 2.5 and 5 vol % at 23 ± 2 °C.

2.4. Viscosity and density measurements

Interfacial mass transfer resistances vary with solution viscosities. In this study, viscosities of nanofluids comprised of a base fluid containing 1 g/L sodium sulfite and 1 mg/L $CoCl_2$ and 0, 0.5, 2.5 and 5% volume fraction SiO_2 nanoparticles were measured using a falling ball viscometer (Cole-Parmer, Vernon Hills, IL, WU-08701-00) at room temperature (23.5 ± 1 °C). Densities were determined from mass measurements using an analytical balance (Thermo Fisher Scientific Inc., Pittsburgh, PA, 01-920-051) for pipetted (Thermo Fisher Scientific Inc., Pittsburgh, PA, 05-403-121) sample volumes from 1–5 mL. Three replicates were conducted for each sample. Measurement procedures were verified with nanopure water. Nanopure water dynamic viscosity was measured at 0.958 mPa s; in close agreement with the literature reference value of 0.97 mPa s [30]. Measured nanopure water density was 998 kg/m^3, close to the reference value of 997 kg/m^3 at 23.5 °C [31].

3. Results and discussion

3.1. Adsorption

Measured chloride concentrations before and after 50 h incubation are shown in Fig. 3. Results above and below the line of parity for the membrane and nanofluid are attributed to experimental
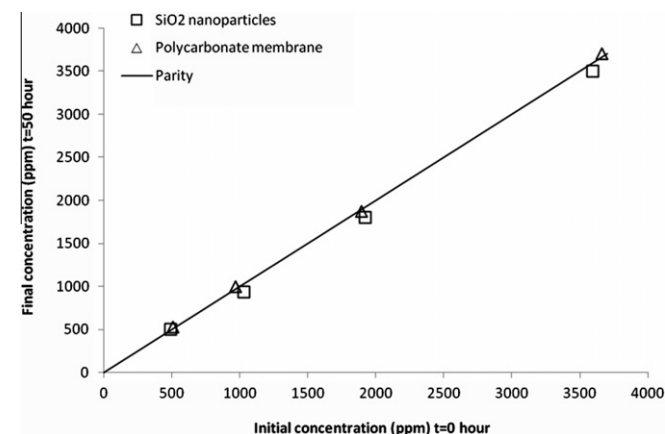
uncertainty. Chloride adsorption is not apparent for the concentrations studied and the results in this study are interpreted for conditions of mass transfer without physical adsorption.

3.2. Viscosity and density

Shown in Fig. 4 are nanofluid dynamic viscosity and density. The density and viscosity increase with increasing SiO_2 volume fraction. The viscosity of 5% nanofluid is 1.3 mPa s. This is 47% higher than that of the base fluid containing no nanoparticles. The well known Einstein correlation [32] can be used to predict solution viscosities of particle suspensions when volume concentration is less than approximately 5%. Using the Einstein correlation, the predicted 5% nanofluid viscosity is 1.0 mPa s, 30% less than the measured value. Failure of the Einstein correlation to predict nanofluid viscosities were reported elsewhere [33–35]. Our measured viscosity value at 5% is lower than that of Tavman et al. [34] who reported a viscosity of 4.3 mPa s for 4.5% SiO_2 nanofluid at 23.5 °C, but similar to that of Nguyen et al. [33] for a 5% 36 nm Al_2O_3 nanofluid who measured a viscosity of 1.5 mPa s at ambient conditions.

3.3. Nanoparticle effects on oxygen transfer

During the experimental trials, the saturated oxygen concentrations necessary to calculate K_La were observed to decrease with increased nanofluid volume fraction for both nanoparticle sizes. To account for slight variations in environmental conditions, saturated oxygen concentrations for controls of 0% volume fraction were also determined on the same day of study for each treatment. Shown in Table 2 are the ratios of C_{sp} for the nanofluid to the nanoparticle free control C_{so} for different volume fractions. For a nanoparticle concentration of 5%, the saturated oxygen concentration is reduced by 7% when compared to a solution without nanoparticles present. Decreasing C_s with increasing nanoparticle volume fraction may be a probe artifact rather than truly lower C_s. Dissolved oxygen probe readings are proportional to the rate of oxygen diffusion to the electrode and the presence of nanoparticles appear to reduce oxygen transfer to the probe tip. While not conclusive evidence, this effect by itself indicates diffusive interfacial mass transfer is not enhanced in the presence of nanoparticles.

Shown in Fig. 5 are oxygen volumetric mass transfer coefficients (K_La) for different volume fractions, and two different nanoparticles sizes. Nanoparticle diameters used are within 5 nm difference, and an effect of nanoparticle sizes on K_La is not apparent in Fig. 5. Thus, when comparing volume fraction effect, an average K_La of

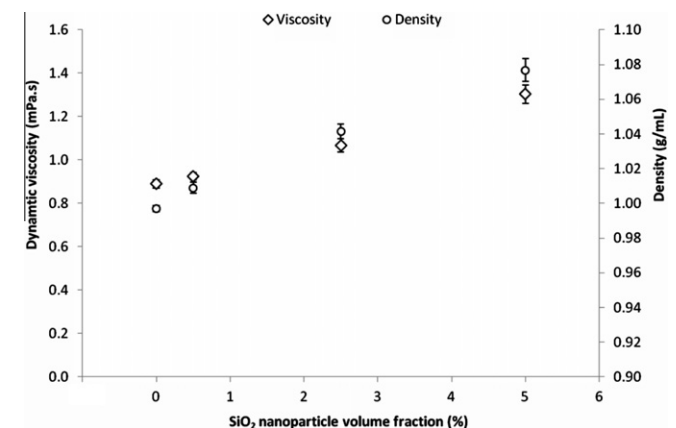
Fig. 3. Comparison of Cl$^-$ concentrations after soaking the polycarbonate membrane or SiO_2 nanoparticles in NaCl over 50 h.

Fig. 4. Dynamic viscosity and density of 0, 0.5, 2.5 and 5% volume fraction SiO_2 nanofluids.

Table 2
The ratio of saturated oxygen concentration (C_{sp}) to the saturated oxygen concentration in the nanoparticle free control (C_{so}) for different volume fraction (%).

Volume fraction (%)	C_{sp}/C_{so}	Standard deviation
0.5	0.99	0.016
2.5	0.95	0.036
5	0.93	0.018
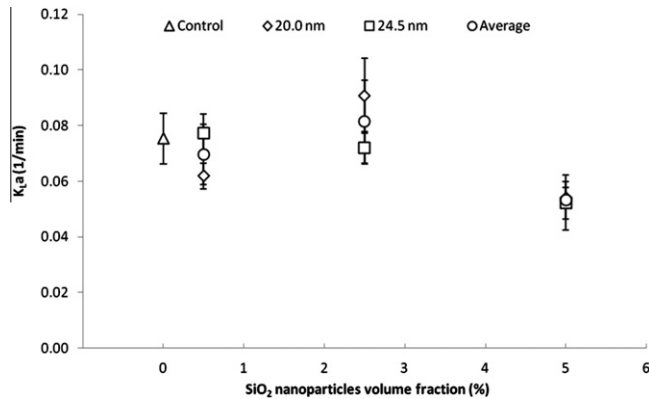
Fig. 5. Oxygen volumetric mass transfer coefficient (K_La) of nanoparticle free control and 0.5, 2.5 and 5% volume fraction SiO$_2$ nanofluids for 20.0 nm, 24.5 nm nanoparticles and average of two different sizes.

both sizes is used for the same volume fraction. The average K_La for the controls, 0.5% and 2.5% are not significantly different. The 5% volume fraction K_La is significantly lower than the control with a 33% reduction.

Reduced mass transfer rates found in this study may be attributed to both an obstruction effect of impermeable nanoparticles and also to nanoparticles increasing solution viscosities. The obstruction effect of nanoparticles on oxygen diffusion within a liquid film can be estimated using the Maxwell equation [36], where the oxygen impermeable nanoparticles can elongate oxygen transfer pathways.

$$\frac{D_{eff}}{D} = \frac{1 - \phi}{1 + \phi/2} \tag{6}$$

where D_{eff} is the effective diffusivity with presence of nanoparticles, D is the diffusivity in solution without nanoparticles. Using Eq. (6), the obstruction effect predicted provides a 7.3% reduction for 5% volume fraction nanoparticles, which cannot account for the 33% reduction in this study. However, nanoparticles influence solution viscosity and liquid film mass transfer coefficients are known to decrease with viscosity increases. In this study, viscosity effects can be estimated using Eq. (7) [37], a dimensionless correlation for predicting liquid film mass transfer coefficients in a similar horizontal diffusion cell and stirring configuration.

$$Sh = 0.0157Re^{1.03}Sc^{1/3} \tag{7}$$

where $Sh = K_Ld/D$, $Re = vd\rho/\mu$, $Sc = \mu/\rho D$, K_L is the liquid film mass transfer coefficient, D is mass diffusivity, d is star-head magnetic stir bar diameter, ρ is density of solution, v is velocity, and μ is solution dynamic viscosity. Measured viscosities and densities are shown to increase with nanofluid volume fraction in Fig. 4. Using Eq. (7) with a viscosity of 1.3 mPa s for 5% nanofluids and viscosity of 0.89 mPa s for the nanoparticle free control provides an estimated 22.4% reduction in the liquid film mass transfer coefficient at 5% volume fraction. This viscosity effect along with the reduction due to diffusion blockage (Eq. (6)) yields a total 30% decrease of the transfer coefficient and it is close, within experimental uncertainty,

to the observed 33% decrease. In this study, any mass transfer benefits associated with nanoparticle Brownian motion, if any exist, are minimal and overshadowed by detrimental viscosity effects.

3.4. Nanoparticle effects on NaCl mass transfer

Shown in Fig. 6 are NaCl mass transfer resistances (R_T) for the control and with 0.5 – 5% volume fractions for two different nanoparticle sizes. No consistent nanoparticle size effect is seen. As volume fraction increases, R_T appears to increase slightly or shows no significant change given the experimental uncertainty. The membrane provides the majority of mass transfer resistance for this configuration; and this resistance is independent of viscosity effects. Hence, significant increases in mass transfer resistance due to viscosity effects are likely to be less apparent than those observed during gas absorption measurements.

3.5. Interpretation of results

Findings of no effect or decreased mass transfer rates for nanofluids in our study is contrary to other studies that report enhanced diffusion or mass transfer in nanofluids [13–15,18]. The reasons for this discrepancy are unclear. Non-enhancement is found even though particle sizes and volume fractions used in this study are similar to studies presented in Table 1. Measurement uncertainty can be dismissed as the cause; the lowest reported mass transfer enhancement from Table 1 is 190% and, based upon a first-order second-moment uncertainty analysis [38], as provided in the Appendix A, our propagated experimental uncertainty is only 6% for the NaCl transfer measurements and only 5% for the oxygen transfer measurements. Particle type may play a role. In this study a silica nanofluid was used and our results are similar to Turanov and Tolmachev [16], who also investigated a silica nanofluid and reported a 25% ^{1}H self-diffusion coefficient reduction at a 23% nanoparticle volume fraction. Why particle type matters is unclear, nanoparticle Brownian motion creating a zone of influence is proposed by others [18,20] to explain enhancement results, but this same motion and effect would be expected independent of particle type. Finally, our measurements were for mass transfer in a non-reactive system and herein may be the true difference. Results in Table 1 for enhanced mass transfer rates are reported exclusively for mass transfer accompanied and enhanced by chemical reaction. How chemical reaction is accounted for may complicate interpretation of results. Komati and Suresh [18] acknowledge interfacial adsorption could contribute to their measured enhancements for nanofluids. Similarly, Ozturk et al. [19] argue that the anomalous enhancement for diffusivities determined from dye diffusion
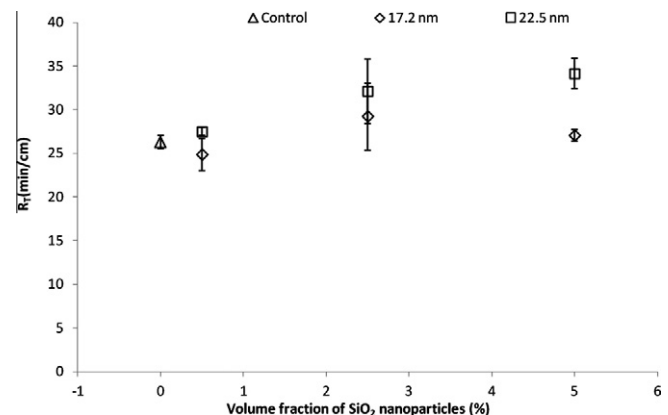
Fig. 6. NaCl mass transfer resistance (R_T) of nanoparticle free control and 0.5, 2.5 and 5% volume fraction SiO$_2$ nanofluids for 17.2 and 22.5 nm nanoparticles.

[13,17] is due to complexation interactions between the dye and nanoparticles. Measurements in this study were not hampered by interpretation of adsorption and reaction enhancements and thus may provide a clearer understanding of the effects of nanoparticles on mass transfer rates.

4. Conclusions

No mass transfer enhancements were found in the presence of nanoparticles for both of oxygen and NaCl mass transfer. Oxygen transfer was actually diminished at the highest nanoparticle volume fraction; this is attributed to solution viscosity effects and the obstruction effect of impermeable nanoparticles. These non-enhanced mass transfer results indicate Brownian motion and micro-convection of nanoparticles cannot be the mechanism controlling heat and mass transfer in nanofluids.

Acknowledgments

Appendix A

1. Experimental uncertainty analysis for NaCl transfer is presented as follows:

$$R_T = -\frac{2A_p}{V \ln \frac{\Delta C_t}{\Delta C_0}} t$$

$$\Delta C_t = C_{ht} - C_{lt}$$

$$\Delta C_0 = C_{h0} - C_{l0}$$

A_p and V are fixed values, error from t is negligible in this study. Thus,

$$R_T = f(C_{ht}, C_{h0}, C_{lt}, C_{l0})$$

The propagated experimental uncertainty is given by:

$$\Delta R_T = \sqrt{\left(\frac{\partial R_T}{\partial C_{ht}}\Delta C_{ht}\right)^2 + \left(\frac{\partial R_T}{\partial C_{lt}}\Delta C_{lt}\right)^2 + \left(\frac{\partial R_T}{\partial C_{l0}}\Delta C_{l0}\right)^2 + \left(\frac{\partial R_T}{\partial C_{h0}}\Delta C_{h0}\right)^2}$$

1.1 For $((\partial R_T/\partial C_{ht})\Delta C_{ht})$,

$$\frac{\partial R_T}{\partial C_{ht}} = \frac{2A_p t}{V} \frac{1}{\ln^2 \frac{\Delta C_t}{\Delta C_0}} \frac{1}{C_{ht} - C_{lt}}$$

$$\Delta C_{ht} = 2\% \times C_{ht} \quad (2\% \text{ is probe reproducibility})$$

Calculations of remaining terms are similar, and

$$\frac{\Delta R_T}{R_T} = 6\%$$

2. Experimental uncertainty analysis for O_2 transfer is presented as follows:

$$K_L a = \frac{\ln\left(\frac{C_s - C_0}{C_s - C_t}\right)}{t}$$

$$K_L a = f(C_s, C_t, C_0)$$

The propagated experimental uncertainty is given by:

$$\Delta K_L a = \sqrt{\left(\frac{\partial K_L a}{\partial C_s}\Delta C_s\right)^2 + \left(\frac{\partial K_L a}{\partial C_t}\Delta C_t\right)^2 + \left(\frac{\partial K_L a}{\partial C_0}\Delta C_0\right)^2}$$

2.1 For $((\partial K_L a/\partial C_s)\Delta C_s)$,

$$\frac{\partial K_L a}{\partial C_s} = \frac{C_0 - C_t}{t(C_s - C_0)(C_s - C_t)}$$

$$\Delta C_s = 1\% \times C_s \quad (1\% \text{ is probe accuracy})$$

Calculations of remaining terms are similar, and

$$\frac{\Delta K_L a}{K_L a} = 5\%$$

References

[1] X.X. Xinwei Wang, Stephen U.S. Choi, Thermal conductivity of nanoparticle-fluid mixture, Journal of Thermophysics and Heat Transfer 13 (1999) 474–480.

[2] S.M.S. Murshed, K.C. Leong, C. Yang, Enhanced thermal conductivity of TiO2–water based nanofluids, International Journal of Thermal Sciences 44 (2005) 367–373.

[3] J.A. Eastman, S.U.S. Choi, S. Li, W. Yu, L.J. Thompson, Anomalously increased effective thermal conductivities of ethylene glycol-based nanofluids containing copper nanoparticles, Applied Physics Letters 78 (2001) 718–720.

[4] J. Garg, B. Poudel, M. Chiesa, J.B. Gordon, J.J. Ma, J.B. Wang, Z.F. Ren, Y.T. Kang, H. Ohtani, J. Nanda, G.H. McKinley, G. Chen, Enhanced thermal conductivity and viscosity of copper nanoparticles in ethylene glycol nanofluid, Journal of Applied Physics 103 (2008) 074301–074306.

[5] M.-S. Liu, M. Ching-Cheng Lin, I.T. Huang, C.-C. Wang, Enhancement of thermal conductivity with carbon nanotube for nanofluids, International Communications in Heat and Mass Transfer 32 (2005) 1202–1210.

[6] M.-S. Liu, M.C.-C. Lin, C.Y. Tsai, C.-C. Wang, Enhancement of thermal conductivity with Cu for nanofluids using chemical reduction method, International Journal of Heat and Mass Transfer 49 (2006) 3028–3033.

[7] A. Sergis, Y. Hardalupas, Anomalous heat transfer modes of nanofluids: a review based on statistical analysis, Nanoscale Research Letters 6 (2011) 391.

[8] S.K.a.A.G.Y. Sezer Özerinç, Enhanced thermal conductivity of nanofluids: a state-of-the-art review, Microfluidics and Nanofluidics 8 (2009) 145–170.

[9] W. Yu, D.M. France, J.L. Routbort, S.U.S. Choi, Review and comparison of nanofluid thermal conductivity and heat transfer enhancements, Heat Transfer Engineering 29 (2008) 432–460.

[10] X.-Q. Wang, A.S. Mujumdar, Heat transfer characteristics of nanofluids: a review, International Journal of Thermal Sciences 46 (2007) 1–19.

[11] V. Trisaksri, S. Wongwises, Critical review of heat transfer characteristics of nanofluids, Renewable and Sustainable Energy Reviews 11 (2007) 512–523.

[12] J.-K. Kim, J.Y. Jung, Y.T. Kang, The effect of nano-particles on the bubble absorption performance in a binary nanofluid, International Journal of Refrigeration 29 (2006) 22–29.

[13] S. Krishnamurthy, P. Bhattacharya, P.E. Phelan, R.S. Prasher, Enhanced mass transport in nanofluids, Nano Letters 6 (2006) 419–423.

[14] B. Olle, S. Bucak, T.C. Holmes, L. Bromberg, T.A. Hatton, D.I.C. Wang, Enhancement of oxygen mass transfer using functionalized magnetic nanoparticles, Industrial & Engineering Chemistry Research 45 (2006) 4355–4363.

[15] H. Zhu, B.H. Shanks, T.J. Heindel, Enhancing CO-water mass transfer by functionalized MCM41 nanoparticles, Industrial & Engineering Chemistry Research 47 (2008) 7881–7887.

[16] A. Turanov, Y. Tolmachev, Heat- and mass-transport in aqueous silica nanofluids, Heat and Mass Transfer 45 (2009) 1583–1588.

[17] X. Fang, Y. Xuan, Q. Li, Experimental investigation of enhanced mass transfer in nanofluids, Applied Physics Letters 95 (2009) 203103–203108.

[18] S. Komati, A.K. Suresh, Anomalous enhancement of interphase transport rates by nanoparticles: effect of magnetic iron oxide on gas-liquid mass transfer, Industrial & Engineering Chemistry Research 49 (2010) 390–405.

[19] S. Ozturk, Y.A. Hassan, V.M. Ugaz, Interfacial complexation explains anomalous diffusion in nanofluids, Nano Letters 10 (2010) 665–671.

[20] J. Veilleux, S. Coulombe, A total internal reflection fluorescence microscopy study of mass diffusion enhancement in water-based alumina nanofluids, Journal of Applied Physics 108 (2010) 104316–104318.

[21] C.H. Li, G.P. Peterson, Mixing effect on the enhancement of the effective thermal conductivity of nanoparticle suspensions (nanofluids), International Journal of Heat and Mass Transfer 50 (2007) 4668–4677.

[22] R. Prasher, P. Bhattacharya, P.E. Phelan, Thermal conductivity of nanoscale colloidal solutions (nanofluids), Physical Review Letters 94 (2005) 025901.

[23] J. Buongiorno, Venerus, et al., A benchmark study on the thermal conductivity of nanofluids, Journal of Applied Physics 106 (2009) 094312–094314.

[24] X. Zhang, H. Gu, M. Fujii, Experimental study on the effective thermal conductivity and thermal diffusivity of nanofluids, International Journal of Thermophysics 27 (2006) 569–580.

[25] M.G. Davidson, W.M. Deen, Hindered diffusion of water-soluble macromolecules in membranes, Macromolecules 21 (1988) 3474–3481.

[26] W.M. Deen, M.P. Bohrer, N.B. Epstein, Effects of molecular size and configuration on diffusion in microporous membranes, AIChE Journal 27 (1981) 952–959.

[27] J.M. Nitsche, G. Balgi, Hindered Brownian diffusion of spherical solutes within circular cylindrical pores, Industrial & Engineering Chemistry Research 33 (1994) 2242–2247.

[28] I.L. Rodrigo Riquelme, Carlos Pérez-López, Juan A. Rayas, Ramón Rodríguez-Vera, Lensless Fourier transform digital holographic interferometer for diffusivity measurement of miscible transparent liquids, Review of Scientific Instruments 80 (2009) 053106.

[29] Y. Kirino, T. Yokoyama, T. Hirono, T. Nakajima, S. Nakashima, Effect of density-driven flow on the through-diffusion experiment, Journal of Contaminant Hydrology 106 (2009) 166–172.

[30] L. Korson, W. Drost-Hansen, F.J. Millero, Viscosity of water at various temperatures, The Journal of Physical Chemistry 73 (1969) 34–39.

[31] P.H. Bigg, Density of water in SI units over the range 0–40°C, Journal of Applied Physics 18 (1967).

[32] A. Einstein, Eine neue Bestimmung der Moleküldimensionen, Annalen der Physik 324 (1906) 289–306.

[33] C.T. Nguyen, F. Desgranges, G. Roy, N. Galanis, T. Maré, S. Boucher, H. Angue Mintsa, Temperature and particle-size dependent viscosity data for water-based nanofluids - hysteresis phenomenon, International Journal of Heat and Fluid Flow 28 (2007) 1492–1506.

[34] A.T.I. Tavman, M. Chirtoc, H.P. Schuchmann, S. Tavman, Experimental investigation of viscosity and thermal conductivity of suspensions containing nanosized ceramic particles, International Scientific Journal 34 (2008).

[35] D.K. Fei Duan, Alexandru Crivoi, Viscosity affected by nanoparticle aggregation in Al_2O_3-water nanofluids, Nanoscale Research Letters 6 (2011).

[36] E.L. Cussler, Diffusion-Mass Transfer in Fluid Systems, Cambridge University Press, New York, 2009.

[37] K. Tojo, J.A. Masi, Y.W. Chien, Hydrodynamic characteristics of an in vitro drug permeation cell, Industrial & Engineering Chemistry Fundamentals 24 (1985) 368–373.

[38] A. Wheeler, A. Ganji, Introduction to Engineering Experimentation, second ed., Prentice Hall, 2003.